A R C H I V E S O F M E T A L L U R G Y A N D M A T E R I A L S
Volume 53 2008 Issue 1

P. OZGA*, Z. ŚWIĄTEK*, M. MICHALEC**, B. ONDERKA*, J. BONARSKI*

PHASE STRUCTURE AND TEXTURE OF ELECTRODEPOSITED InSn ALLOYS ON COPPER SUBSTRATE

STRUKTURA FAZOWA ORAZ TEKSTURA OSADZONYCH ELEKTROLITYCZNIE STOPÓW InSn NA PODŁOŻU MIEDZIANYM

The In-Sn alloys are interesting as the materials used in the lead-free interconnection technology and as the replacement materials for toxic cadmium layers. This work investigated the indium-tin layers electrodeposited from the complex citrate solutions. The citrate electrolytic baths are especially attractive as the non-toxic baths for the electrodeposition of alloys. The depositions were conducted in various hydrodynamic conditions by means of the rotating disc electrode technique (RDE). It was observed that the applied potential, hydrodynamic conditions, pH, composition of solution and additional organic compounds have a strong effect on the chemical composition, the phase structure and the texture of the electrodeposited layers. The phase equilibria in the Cu-In-Sn ternary system were calculated and the isopleths of the phase diagram were presented. The X-ray structural investigations of the thermal stability of the deposits on the copper substrate were carried out in the temperature range from 25 to 400°C.

Keywords: Lead-free alloys, InSn alloy, electrodeposition, phase structure, texture, citrate bath, Cu-In-Sn phase diagram

Stopy In-Sn są interesujące jako materiały dla technologii połączeń bezołowiowych oraz jako materiały zastępujące toksyczne warstwy kadmowe. W pracy badano warstwy indowo-cynowe osadzone z kompleksowych roztworów cytrynianowych. Kąpiele cytrynianowe są szczególnie atrakcyjne jako nietoksyczne kąpiele dla elektrolitycznego osadzania stopów. Osadzanie prowadzono w różnych warunkach hydrodynamicznych przy zastosowaniu wirującej elektrody dyskowej (WED). Stosowany potencjał, warunki hydrodynamiczne, pH, skład roztworu i dodatki składników organicznych miały silny wpływ na skład chemiczny, strukturę fazową i teksturę osadzonych warstw. Obliczono równowagi fazowe w układzie Cu-In-Sn i przedstawiono izoplety diagramu fazowego. W zakresie 25 do 400°C przeprowadzono badania termicznej stabilności osadów na podkładzie miedzianym przy zastosowaniu strukturalnej analizy rentgenowskiej.

1. Introduction

The In-Sn alloys are especially interesting as the materials used for the lead-free interconnection technology (diffusion soldering) [1,2] and as the replacement materials for toxic cadmium layers (high corrosive resistance, similar to the cadmium layers) [3]. The electrodeposition technique has significant advantages to the other methods of deposition of InSn layers, which are: (i) the low temperature of the deposition, (ii) the relatively low losses of metals (indium is expensive) (iii) the accurate control of the thickness of the layer. Citrate electrolytes are attractive as non-toxic baths for the electrodeposition of metals, alloys and semiconductor materials [4, 5, 6]. Citrates form complexes with In(III) and Sn(II). On this account, citrate baths can be prepared for electrodeposition of binary In-Sn alloys. The kind of electrolyte can have a great influence on the properties and the phase composition of the electrodeposited layers [5]; hence, the analysis of the phase structure, the thermal stability of the deposits on the copper substrate and the texture of the electrodeposited InSn alloys can be very important for the application of these layers in diffusion soldering or in anticorrosive coating.

2. Experimental procedure

The electrolysis was carried out in 100 ml and 500 ml cell with rotating disk electrode (RDE) to ensure constant and controlled hydrodynamic conditions. The temperature of electrolytes was maintained at 20°C±0.2°C. Redestillated water was used for the preparation of the solutions, from which gases had been removed by boiling. The preparation of the solution and the experiments

* INSTITUTE OF METALLURGY AND MATERIALS SCIENCE OF THE POLISH ACADEMY OF SCIENCES, 30-059 KRAKÓW (CRACOW) REYMONTA 25, POLAND
** FACULTY OF CHEMISTRY, JAGIELLONIAN UNIVERSITY, INGARDENA 3, 30-060 KRAKÓW (CRACOW) POLAND

on the solutions were performed in argon atmosphere (Argon 5.0, Air Products). The system was supplied by a PAR 273A EG&G potentiostat-galvanostat. Polycrystalline copper disks (0.071 cm^2 – in partial polarization measurements and 2.73 cm^2 – in the preparation of the samples for the X-ray structural and texture analysis) rotating at 0 – 68 rad/s were applied as the cathode. The copper electrodes were chemically polished with the use of a mixture of concentrated nitric, acetic and phosphoric acids (1:1:1) in the ambient temperature. A Sn rod ($5cm^2$) was used as the anode. The cathode potentials were referred to a saturated calomel electrode (SCE) and were corrected for ohmic drop (CI method). The potential scan rate was v = 2 mV/s in potentiodynamic experiments. The chemical composition and the mass of the deposits were determined by the EDS analysis with the use of the LINK-ISIS system attached to the Philips XL 30 Scanning Electron Microscope. The analysis was carried out within the scanned area of about 1 mm^2. The tin coatings on the copper substrate were used as the standards for the determination of the absolute mass of the coatings in a similar way to the one in the earlier works [7, 8]. The mass of the coating was used for the calculation of the current efficiency and the partial polarization curves. The useful linear range was found to be from 0 to about 50 μg Sn at 28 kV accelerating voltage. This linearity was the basis for the assumption that in the case of the In-Sn coatings, the correlation between the relative intensities of $(I_{Sn} + I_{In})/(I_{Cu} + I_{Sn} + I_{In})$ and the mass of In-Sn deposit would be analogous to that of the Sn standards $I_{Sn}/(I_{Sn} + I_{Cu})$.

The X-ray diffractometry, with the use of the Philips diffractometer type X'Pert PRO in the Bragg-Brentano geometry, was used to identify the phase composition in the deposits of different In concentrations. CuKα radiation (wavelength λ = 0.154184 nm) diffracted by sample was selected by means of a graphite monochromator. The scanning voltage of the X-ray tube was 40 kV, the current was 25 mA, the exposure time was 10 s and the measured angle, 2θ, was from 25° to 95°. The scanning step was 0.02°. The high temperature X-ray diffraction studies were carried out using the reaction chamber type XRK 900 (Anton Paar). The sample was heated from 25°C up to 400°C in air with the step of 25°C. The measured angle, 2θ, was from 26° to 48° with the scanning step of 0.02°. The lattice parameters were determined by means of the Philips X'Pert Plus software for all the detected peaks.

The texture measurements were performed with the application of the Philips X'Pert system, equipped with the texture goniometer ATC-3. The filtered X-ray radiation CoKα (wavelength λ = 0.179026 nm) was used. The incomplete pole figures were registered by means of the Schulz back-reflection technique [9], for the following ranges of the radial (α) and azimuthal (β) angles: α = 0° to 75° and β = 0° to 360°, with steps Δα = 5° and Δβ = 5°, respectively.

3. Results and discussion

3.1. Optimal citrate baths compositions and electrolysis conditions for the electrodeposition of In-Sn alloys

The initial investigations of the electrodeposition of the In-Sn alloy were conducted in the citrate bath described by Zorkina et al. [10]. These investigations showed the lack of stability of this bath. The precipitates of hydroxides and insoluble citrates were present in the solution after several hours. Hence, in our investigations, the optimal citrate bath composition was determined on the basis of thermodynamic analysis of the In(III)-Sn(II)-Cit system (where Cit denote $C_6H_4O_7^{-4}$) and on the basis of the polarization experiments. The VCS (Villars – Cruise – Smith) algorithm was used in the calculations of the equilibrium concentrations [11]. Citrate baths for In(III)-Sn(II)-Cit (where Cit denote $C_6H_4O_7^{-4}$) are not stable for a pH lower than about 2.4, as the formation of the citrate complexes as dominate species of Sn(II) starts above a pH of about 2. Below pH 2.4, precipitates of $Sn(OH)_2$ and citrate polymers $[SnH_2Cit^o]_n$ are possible. On that account, the citrate baths have limited stability. The current efficiency of indium electrodeposition diminishes with the increase of pH above 2.6; hence, the optimal pH range for the electrodeposition of the In-Sn alloys is between 2.4 and 2.6. The decay of the current efficiency of the indium electrodeposition on the cathode above pH 2.6 is connected with the formation in the solutions of the predominant electrochemically non-active indium citrate complexes with a high negative charge: $[In(HCit)_2]^{-3}$ and $[In_3(OH)(Cit)_3]^{-4}$. The baths at pH 2.5 were also well buffered by the citrate ions; hence the little change in the concentration of the solution component, not causing any great changes in the properties of the electrolytes. A strong influence of the anions was stated. The electrodepositon process was activated by the presence of chloride ions in the bath. On the partial polarization curves of indium, strong maxima were observed of the potential from −690 to −800 mV vs SCE, where also observed were the maximal contents of indium in the In-Sn alloys. The optimal potential ranges for the alloy electrodeposition were found in the range from −705 to −750 mV vs SCE, where the content of indium in the alloy was constant. The composition of the alloys depends on the concentration of the citrate ions in solu-

TABLE 1

The chemical composition of the optimal citrate electrolytes for the electrodeposition of In-Sn alloys

No	The electrolyte composition [mol/dm^3]					pH
	$InCl_3$	$SnCl_2 \cdot H_2O$	NH_4Cl	PEG 3000	Citrate ($H_4Cit + Na_3HCit$)	
1	0.07	0.02	0.8	0.0001	0.09	2.5
2	0.09	0.02	0.8	0.0001	0.11	2.5
3	0.11	0.02	0.8	0.0001	0.13	2.5
4	0.13	0.02	0.8	0.0001	0.15	2.5

tion. The increase of the ratio of the citrate concentration to the sum concentrations of the metals (i.e. In(III) and Sn(II)) higher than 1 led to the decreases of the indium content in the alloys, while the decreases of this ratio to below 1 led to the instability of the solution (formation of hydroxides precipitates). Hence, the optimal citrate concentration is close to the sum concentrations of indium(III) and tin(II) in the solution. A positive effect of the polyethylene glycol with the average molecular mass 3000 (PEG-3000) on the quality of the deposits was stated. The baths containing antioxidants (ascorbic acid and pyrogallol) had a limited stability for about 1 week. The chemical compositions of the optimal electrolytes are given in Table 1. The indium content in the In-Sn alloy increases with the increase of the indium(III) concentration in the electrolytic bath from 48 at.% in the deposit obtained from the solution '1' (Tab. 1) to 60 at.% in the deposits obtained from the solution 3 (rotation rate of disc electrode 14 rad/s). A strong influence of the hydrodynamic condition was also stated. The analysis of the polarization curves indicates that the limitations of the partial tin currents by the mass transport of Sn(II) species to the cathode can explain the strong effect of the hydrodynamic conditions on the composition of the In-Sn alloy. The increase of the rotation rate of the disc electrode led to the increase of the tin content in the alloys. For example, the increase of the rotation rate of the disc electrode from 0 rad/s (non-stirred solution) to 68 rad/s led to the increase of the tin content in the alloys by about 100% (from 34 to 67.5 at.%) for the electrodepositon made from the solution 4.

3.2. Thermodynamic properties of phases in Cu-In-Sn system

The electrodeposited alloys may differ considerably in their phase constitution in comparison with the alloys of the same chemical composition but obtained by thermal methods [12]. In the case of the electrodeposited alloys, the metastable phases are often present in the deposits or, for that matter, the phases which have different compositions for the solubility limits [5, 12]. Hence, for the electrodeposited alloys, the phase structure may differ from the phase structure for the equilibrium conditions. In the case of soldering processes, the creation of phases as a result of the reaction of the In-Sn alloy layer with the copper substrate takes place. On this account, the analysis of the phase diagram in the Cu-In-Sn system can be very helpful.

Observations of the phase equilibria in the Cu-In-Sn system have been carried out, among others, by:

1. Koster *i in.* [13] (isothermal sections and, so called, isopleths – vertical sections) – with the use of DTA and metallographic methods
2. Liu *i in.* [14] (8 isothermal sections and 7 vertical sections within the temperature range form 110 to 900°C and the composition range from 10 to 70% mas. Cu) – metallographic methods, XRD and DSC. A range from the Cu-In system to the Cu-Sn system of the homogeneity of the η phase was detected and the presence of a new ternary Cu_2In_3Sn phase at the temperature of 110°C was stated.

The results of the Liu *i in.* [14] investigations show a very high solubility of indium in the $\varepsilon(Cu_3Sn)$ and $\delta(Cu_{41}Sn_{11})$ phases of the Cu-Sn system and a high solubility of tin in the γ and $\delta(Cu_7In_3)$ phases of the Cu-In system.

On the basis of the literature data and the own data, Liu *i in.* [14] conducted a critical analysis of the data and the thermodynamic modelling of the equilibria in the Cu-In-Sn system, by means of the CALPHAD method (**Cal**culation of **Pha**se **D**iagram) [15]. The list of solid phases in the ternary Cu-In-Sn system have been collected in Table 2.

For the determination of the vertical sections (isopleths) of the phase diagram presented in this paper (Figure 1-3), the model parameters from the COST531 (ver.2.0) data base were applied, after minor corrections. The phase diagrams were calculated with the use of the PANDAT (ver. 7) software.

TABLE 2

Solid phases in the ternary Cu-In-Sn system

Phase The denotations used in ternary system*	Phase The denotations used in binary system	Prototype (Structure)[10]	Model
Cu_2In_3Sn ξ	–	Cu_2In_3Sn	$(Cu)_{0.333}(In)_{0.5}(Sn)_{0.167}$
$Cu_{77}(In,Sn)_{23}$, $Cu_{10}(In,Sn)_3$ ζ $Cu_{10}Sn_3$	–	$Cu_{10}Sn_3$	$(Cu)_{0.77}(In,Sn)_{0.23}$
(Cu) (FCC)	(Cu)/FCC	Cu (A1)	(Cu,In,Sn)
β (BCC)	β (Cu-In)	W (A2)	(Cu,In,Sn)
βSn (Sn)	βSn	βSn (A5)	(Cu,In,Sn)
(In)	(In)	In (A6)	(Cu,In,Sn)
η CuIn_η $Cu_6(Sn,In)_5$, Cu(InSn)_η	η(Cu-In)	NiAs ($B8_1$)	$(Cu)_{0.545}(Cu,In,Sn)_{0.122}(In,Sn)_{0.333}$
CuIn_η' $Cu_2(In,Sn)$	η'(Cu-In)	Ni_2In ($B8_2$)	$Cu_{0.64}In_{0.36}$
ε Cu_3Sn,$Cu_3(In,Sn)$	ε(Cu-Sn)	Cu_3Sn	$Cu_{0.75}(InSn)_{0.25}$
δ $Cu_{41}Sn_{11}$, $Cu_{41}(In,Sn)_{11}$ CuSn_δ	δ(Cu-Sn)	$Cu_{41}Sn_{11}$	$Cu_{0.788}(In,Sn)_{0.212}$
CuIn_δ $Cu_7(In,Sn)_3$	δ(Cu-In)	Cu_7In_3	$Cu_{0.7}(In,Sn)_{0.3}$
CuIn_γ	γ(Cu-In)	$InMn_3$	$C_{0.654}(Cu,In)_{0.115}(In,Sn)_{0.231}$
InSn_γ	γ(In-Sn)		(In,Sn)
InSn_β	β(In-Sn)	In (A6)	(In,Sn)
$Cu_{11}In_9$,θ CuIn	θ(Cu-In)	AlCu	$Cu_{0.55}In_{0.45}$

* denotations used in this and other papers

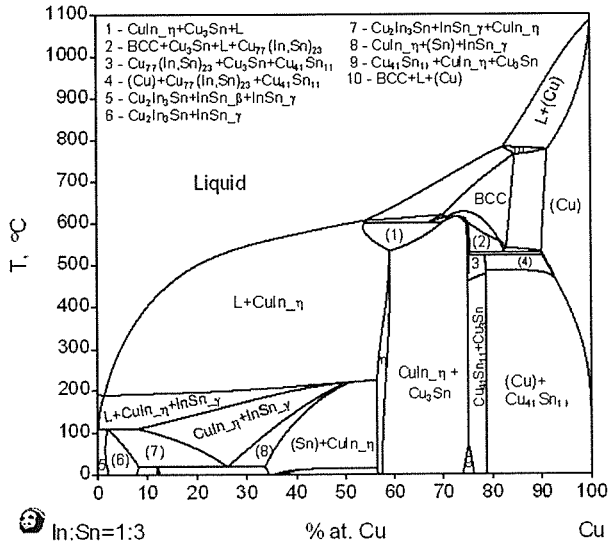

Fig. 1. The T-X section of the phase diagram for the Cu-In-Sn system calculated for the In:Sn ratio 1:3

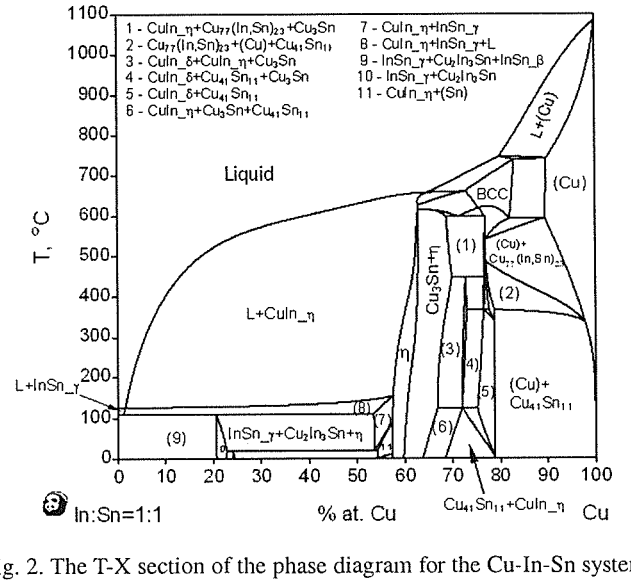

Fig. 2. The T-X section of the phase diagram for the Cu-In-Sn system calculated for the In:Sn ratio 1:1

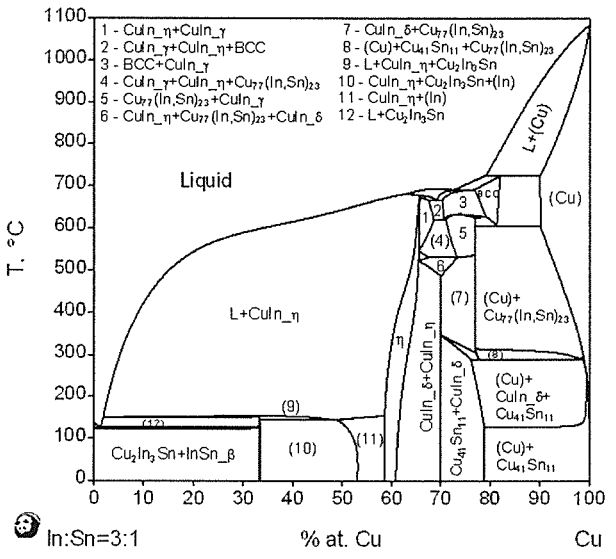

Fig. 3. The T-X section of the phase diagram for the Cu-In-Sn system calculated for the In:Sn ratio 3:1

3.3. X-ray structural investigations

3.3.1. Structure of deposited alloys

Figure 4 presents the results of X-ray structural investigations on the Sn-In deposits within the concentration range of indium from 21.5 to 81.6 at% In and temperature 25°C. From the analysis of the X-ray diffraction patterns it is evident that electrodeposited Sn-In alloys exhibit two phases: the InSn_γ phase with a simple hexagonal structure and the InSn_β phase, with a tetragonal one. It can be seen that the β-phase exists in the whole composition range and the γ-phase – up to the deposit containing 66.4%at. In. The deposits with 21.5 and 22.9% at. In contain the β-phase out of the equilibrium limit. Simultaneously, some distinct changes in the peak intensities of the diffraction patterns of the γ phase were identified. A decreasing fraction of the γ phase, and an increasing fraction of the β one, accompanied by an increasing In content in the deposits, was observed. Additionally, along with the increasing In content in the deposits, a shift of the diffraction peaks took place. It can be explained by the changes in the lattice parameters of both phases. The replacement of Sn by In in the hexagonal cell leads to a gradual increase in the cell parameters *a* and *c*. The evolution of the lattice parameters of the γ-phase against the In content in the deposits is shown in Fig. 5a. In the case of the β-phase, substitution of tin by indium atoms with a greater atomic radius (r_{Sn} = 0.172 nm, r_{In} = 0.200 nm) leads to a faster decrease in the cell parameter *a* and increase in *c* (Fig. 5b). For the deposit with the highest In content (81.6% at. In) the phase composition changes, beside the dominating β-phase, a small amount of a CuIn (Database ICCD, PDF No 00-035-1150, [16]) one, with a monoclinic structure is observed.

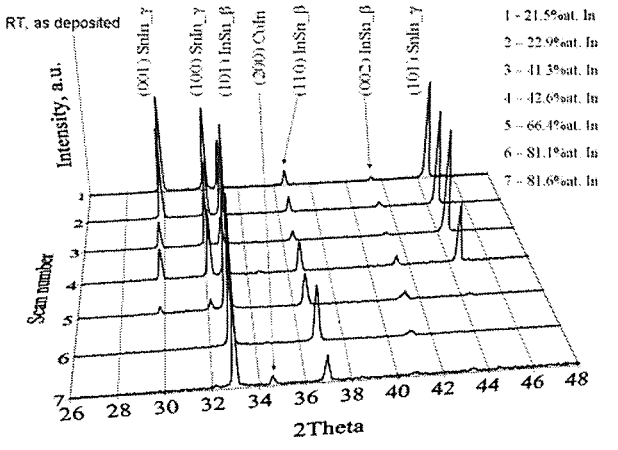

Fig. 4. The X-ray diffraction patterns of the coatings against the indium content in the deposits

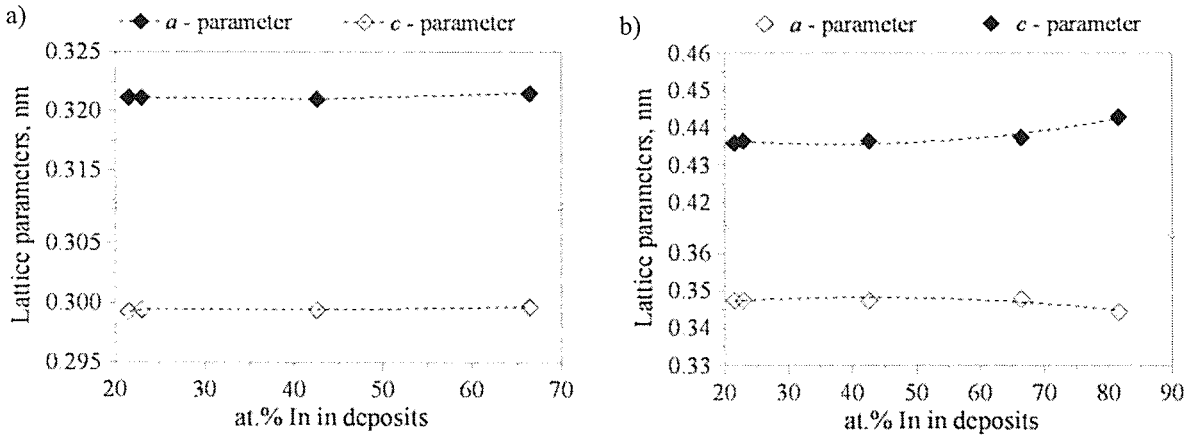

Fig. 5. The variation of the lattice parameters of the hexagonal γ-phase (a) and the tetragonal β-phase (b) versus the indium content in the deposits

3.3.2. Thermal stability

The X-ray structural investigations of thermal stability of deposits were carried out in the temperature range 25 to 400°C according to heating curve visible in Fig. 6. The X-ray diffraction patterns of the coatings against the temperature are shown in Fig. 7. From results obtained, it can be seen that the γ-phase exists in the deposits up to 175°C but from 150°C – only for the deposits with a low indium content (up to 22.9% at. In, see Fig. 7a-b). Simultaneously, for the deposits with a greater In content, only the monoclinic CuIn phase(Database ICCD, PDF No 00-035-1150, [16], phase not present in phase diagram) was observed (Fig. 7h). The diffraction peaks of the β-phase are observed only up to temperature of 125°C, but only in the case of the deposits with a higher indium percentage (from 41.3% at. In, see Fig. 7c-g). The variation of the lattice parameters of both phases dominated in this temperature range versus the indium content in the deposits and the temperature is presented in Fig. 8.

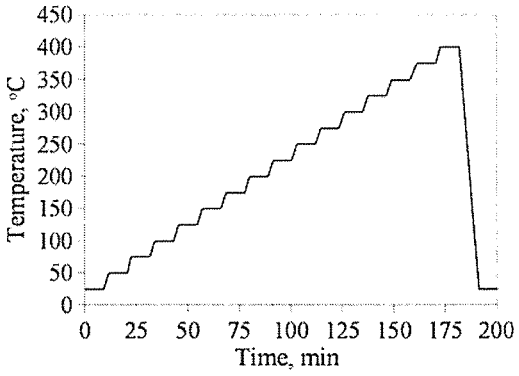

Fig. 6. The heating curve used in the thermal stability investigations

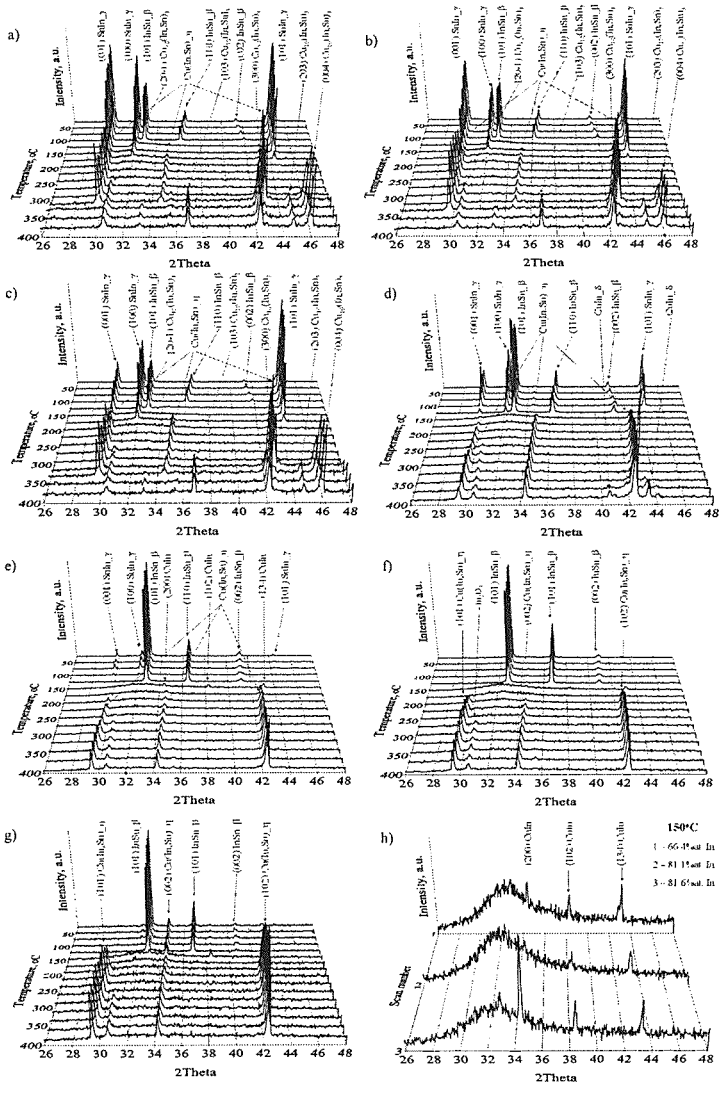

Fig. 7. The recorded X-ray diffraction patterns versus the temperature of the InSn deposits within the concentration range of indium from 21.5 to 81.6% at In (a – 21.5% at. In, b – 22.9% at. In, c – 41.3% at. In, d – 42.6% at. In, e – 66.4% at. In, f – 81.1% at. In, g – 81.6% at. In, h – the phase composition of the deposits with a high In concentration at 150°C)

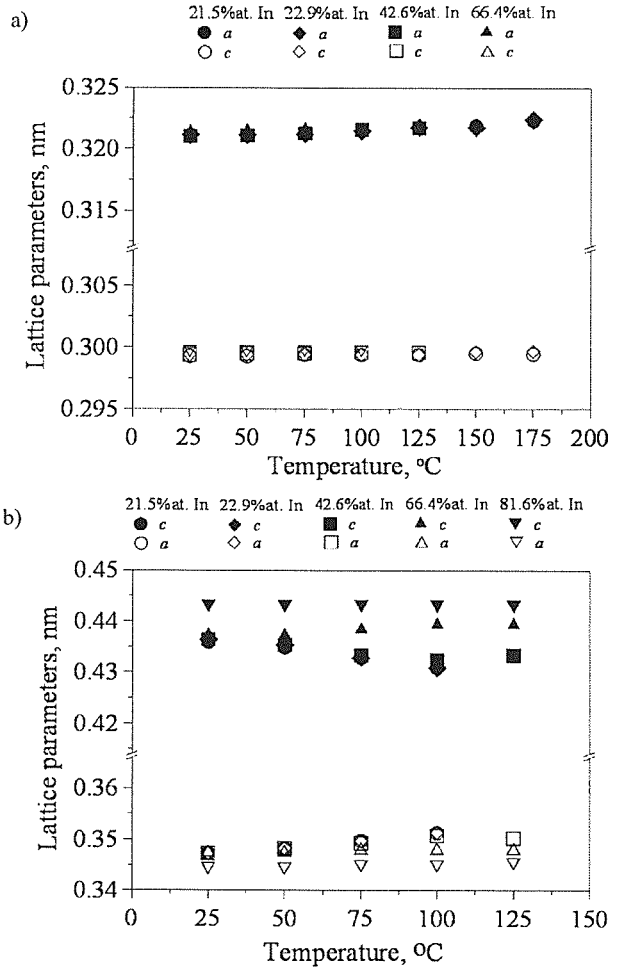

Fig. 8. The variation of the lattice parameters of the hexagonal γ-phase (a) and the tetragonal β-phase (b) versus the indium content in the deposits and the temperature

Along with the increasing the temperature, instead of the CuIn phase a new Cu(In,Sn)_η phase with structure type Cu_2In crystallizes. At the same time, a shift of the diffraction peaks take place what can be explained by the growth of lattice parameters of the Cu(In,Sn)_η phase. At 300°C, for the deposits with a low indium content (21.5% at. In) a new Cu-In-Sn phase: $Cu_{10}(In,Sn)_3$ with a hexagonal structure type $Cu_{10}Sn_3$, crystallizes. It should be noted that the diffraction patterns of this high-temperature phase do not vary up to 400°C.

An increase of the indium content in deposits results in a modification of the phase composition. For 42.6% at. In (Fig. 7d), beside the indium oxide, a triclinic CuIn_δ ($Cu_7(In,Sn)_3$) type Cu_7In_3 is observed. For the deposits with higher indium percentage, from 42.6% at. In (see Fig. 7e-g), the hexagonal Cu(In,Sn)_η phase type Cu_2In is still dominated.

3.4. Effect of Electrodeposition Conditions on the Crystallographic Texture of Indium Tin Alloys Deposits

The sets of incomplete pole figures (100),(001) for InSn_γ (hexagonal structure) and (101), (110) for InSn_β phase (tetragonal structure) were registered. A similar set of incomplete pole figures {111}, {100} and {110} was also registered for the copper substrate. In order to calculate the orientation distribution function (ODF) and the complete pole figures (i.e. for the range of the polar angle from 0° to 90°) the ADC method was used [17] The numerical analysis was performed with the use of the software package LaboTex [18].

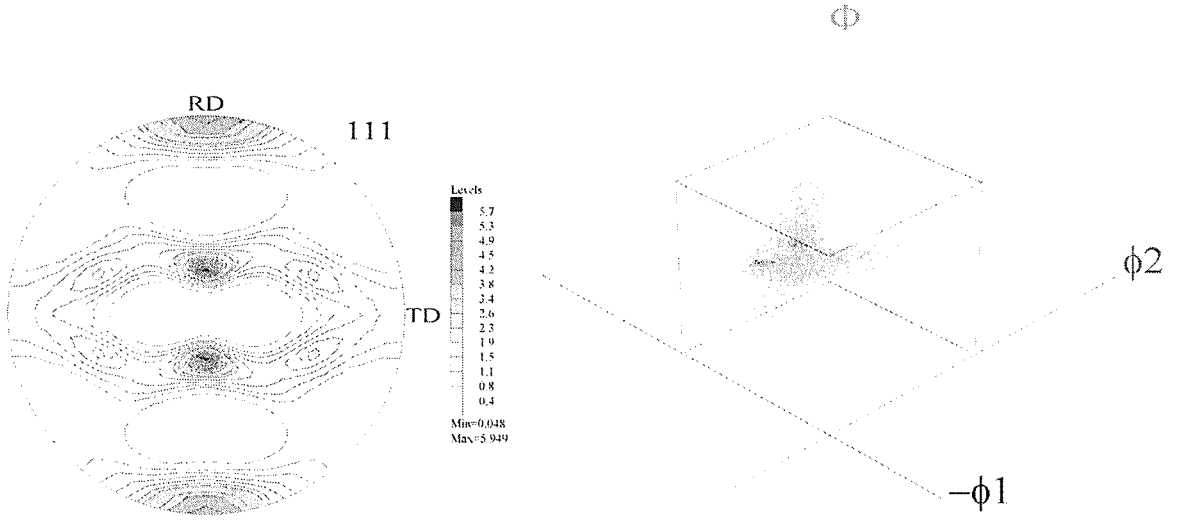

Fig. 9. The pole figure {111} and the ODF of a copper substrate (cathode)

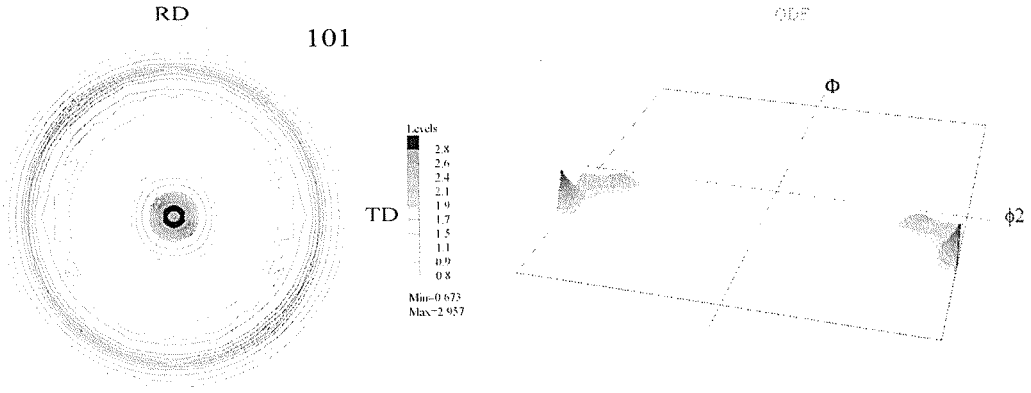

Fig. 10. The pole figure (101) and the ODF (axial symmetry) of the deposit (phase InSn_β). A stirred solution (ω = 14 rad/s)

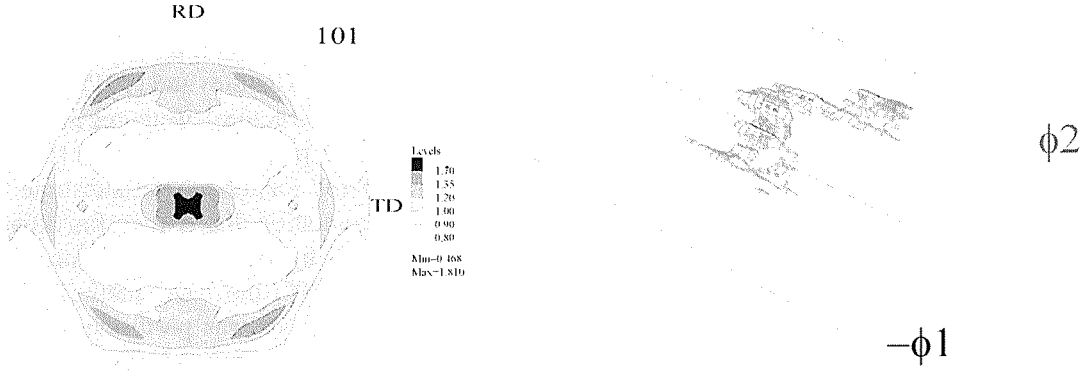

Fig. 11. The pole figure (101) and the ODF of the deposit (phase InSn_β). A non-stirred solution (ω = 0 rad/s)

The texture of the copper substrate is typical for rolling copper. The pole figure {111} and the ODF for the copper substrate (cathode) are presented in Fig. 9. The hydrodynamic conditions have a strong effect on the texture of the In-Sn deposits. The axial texture of the deposits was formed in stirred solutions in both the InSn_γ and InSn_β phases. The dominating texture components in the InSn_γ phase were the fibers {120}||ND, {301}||ND and {212}||ND, while for the InSn_β phase, the fiber {101}||ND was found. An example of the pole figure (101) and the ODF for the phase InSn_γ of the deposit in a stirred solution is presented in Fig. 10. The deposits obtained from the non-stirred solutions during the electrodeposition have a non-axial texture. The dominating texture components in the InSn_γ phase were {103}< −3 − 91 > and the fiber {301}||ND, while in the InSn_β phase, the dominating one was {231}< 1 − 11 >. An example of the pole figure (101) and the ODF for the phase InSn_β of the deposit in a non-stirred solution is presented in Fig. 11.

4. Conclusion

- It was provided that the In-Sn alloys can be obtained by electrodeposition from stable citrate solutions.
- The analysis of thermodynamic models of citrate systems and the results of electrochemical activity of the citrate complexes make it possible to indicate a very narrow range of pH – from 2.4 to 2.6 – of the solution as optimal for the electrodeposition of indium-tin alloys. Also stated was a positive influ-

ence of the presence of chloride ions as well as PEG 3000, in the solution.

- The plateaus of the maximal content of indium in the In-Sn alloys were obtained in the range from –705 to –750 mV vs SCE. A strong influence of the hydrodynamic condition on the contents of indium in the alloys was stated. A lowered rotation rate of the disk electrode raises the indium content in the alloy.
- The electrodeposited Sn-In alloys exhibit two phases: the InSn_γ phase, with a simple hexagonal structure, and the InSn_β phase, with a tetragonal one. The deposits contain also the β-phase out of the equilibrium limit. A small amount of the CuIn phase, with a monoclinic structure, is observed, beside the dominated β-phase, for the deposit with the highest In content (81.6% at. In).
- γ-phase exists in the deposits up to 175°C, but from 150°C – only for the deposits with a low indium content, while, for the deposits with a greater In content, only the monoclinic CuIn phase was observed. The diffraction peaks of the β-phase are observed only up to the temperature of 125°C. At a higher temperature, also observed were the Cu(In,Sn)_η , $Cu_{10}(In,Sn)_3$ and $Cu_7(In,Sn)_3$ phases, as well as some oxides.
- The hydrodynamic conditions have strong influence on the texture of the In-Sn deposits. The axial texture of deposits was formed in stirred solutions.

Acknowledgements

This work was supported by grant from MNISW (Poland) : 3 T08A 04527.

REFERENCES

[1] S. Sommadossi, W. Gust, EJ Mittemeijer, "Characterization of the Reaction Process in Diffusion-Soldered Cu/In-48 at.% Sn/Cu Joints", Mat. Chem. Phys., **77**, (2003) 924.

[2] J. Wojewoda, P. Zięba, B. Onderka, R. Filipek, P. Romanów, "Growth Kinetics of the Intermetallics Formed in Diffusion Soldered Interconnections", Arch.Metall.Mat. **51**, (2006) 345.

[3] E. W. Brooman, "Corrosion Behaviour of Environmentally Acceptable Alternatives to Cadmium and Chromium Coatings: Cadmium", Met.Finishing, April, (2000) 42.

[4] E. Beltowska-Lehman, P. Ozga, "Effect of complex formation on the diffusion coefficient of Cu(II) in citrate solution containing Ni(II) and Mo(VI)", Electrochim. Acta, **43** (1998) 617.

[5] E. Beltowska-Lehman, P. Ozga, Z. Swiatek, C. Lupi, "Influence of structural factor on corrosion rate of functional Zn-Ni coatings", Cryst. Eng., **5** (2002) 335.

[6] E. Beltowska-Lehman, P. Ozga, "Electrodeposition of ZnTe thin films", Arch.Metall.Mat., **50** (2005) 319.

[7] P. Ozga, "Electrodeposition of Sn-Ag and Sn-Ag-Cu alloys from the thiourea solutions", Arch.Metall.Mat. **3** (2006) 413.

[8] P. Ozga, E. Bielańska, "Determination of corrosion rate of Zn and Zn-Ni layers by the EDS technique", Mat. Chem.Phys., **81**, 562-565 (2003).

[9] L. G. Schulz, "A Direct Method of Determining Preferred Orientation of a Flat Reflection Sample Using a Geiger Counter X-Ray Spectrometer", J. Apply. Phys., **20**, (1949) 1030.

[10] O. V. Zorkina, Y. P. Perelygin, "Electrodeposition of tin-indium alloy from citrate electrolyte", Russian Journal of Applied Chemistry , **72** (1999) 1476.

[11] W. R. Smith, R. W. Missen, "Chemical Reactions Equilibrium Analysis : Theory and Algorithms", John Wiley & Sons, Toronto (1982).

[12] P. L. Cavallotti, L. Nobili, A. Vicenzo, "Phase structure of electrodeposited alloys", Electrochimica Acta **50** (2005) 4557.

[13] W. Koster, T. Godecke, D. Heine, Z. Metallkde. **63**, 802 (1972).

[14] X. J. Liu, H. S. Liu, I. Ohnuma, R. Kainuma, K. Ishida, S. Itabashi, K. Kameda, K. Yamaguchi, "Experimental Determination and Thermodynamic Calculation of the Phase Equilibria in the Cu-In-Sn System", J.Electronic Mater., **30**, (2001) 1093.

[15] H. L. Lukas, S. G. Fries, B. Sundman, "Computational Thermodynamics, The Calphad Method", Cambridge University Press, 2007 (ISBN 978-0-521-868811-2).

[16] V. Simic, J. Marinkovic, Less-Common. Met., **72**, 133 (1980).

[17] K. Pawlik, "Determination of the Orientation Distribution Function from Pole Figures in Arbitrarily Defined Cells". Phys. Stat. Sol. (b) **134**, (1986) 477.

[18] K. Pawlik, P. Ozga, "LaboTex: The Texture Analysis Software", Göttinger Arbeiten zur Geologie und Paläontologie, **SB4**, 146-147 (1999).

Received: 3 December 2007.